Finite-Element Analysis of Polyhedra under Point and Line Forces in Second-Strain Gradient Elasticity

Jörg Christian Reiher[1]; Ivan Giorgio, Ph.D.[2]; and Albrecht Bertram[3]

Abstract: In this paper, a finite-element implementation of linear second-strain gradient elasticity is introduced based on a Hellinger-Reissner variational principle in order to use standard finite-element methods. Displacement boundary conditions are applied to one or more vertices of different polyhedrons. As a result, a smooth deformation around deformed vertices of the polyhedrons can be observed, in contrast to the appearance of singularities in the first-order theory, i.e., a Cauchy continuum, where strain singularities appear in such cases.
DOI: 10.1061/(ASCE)EM.1943-7889.0001184.

Author keywords: Strain gradient elasticity; Finite-element method; Line force; Point force.

Introduction

The concepts of point forces and force distributions along lines are often used in mechanics to describe external actions acting possibly on corners and edges of a body, provided that the body has a suitable boundary, i.e., is piecewise smooth. However, the common approach of a Cauchy continuum, i.e., a continuum equipped with an elastic energy that depends on the gradient of its displacement, cannot sustain such point and line forces. A prescription of such boundary conditions along edges or on corners results in singularities of the displacement field. If one wants to marry the idea of a continuum with that of corner and edge forces (or imposed displacements at corners and edges), one has to generalize the concept of the Cauchy continuum. Such a type of generalization appears today especially useful because fast-developing computer-aided manufacturing methods allow the fabrication of very complex microstructures that can sustain suitable external forces applied on the elementary cell and other forms of external actions whose equivalent in the homogenized limit is not within the scope of Cauchy elasticity (dell'Isola et al. 2015c). Extending the elastic energy of the continuum to second and third gradients of the displacement clearly lends itself to this purpose. Since the pioneering works by dell'Isola et al. (2014, 2015a), it is known that higher gradients can be introduced to continuum mechanics. Some relevant papers that should be also mentioned in the framework of linear elastodynamics considering the strain energy density depending on the gradients of the displacement up to the third order are, e.g., those by Mindlin (1972), Agiasofitou and Lazar (2009), and Lazar (2013). In addition, Bertram (2015, 2016a) showed how a constitutive thermodynamical framework for strain gradient elasticity and plasticity can be set up. From the extensions of the studies by Mindlin (1965) and Germain (1973) that have been derived in Javili et al. (2013), Alibert et al. (2003), and dell'Isola et al. (2015b), it is very clear why the introduction of the first-strain and second-strain gradients allow a continuum to sustain boundary conditions on vertices and edges of a body. In the present work, a finite-element approach is presented that allows the integration of displacement gradients up to the order of three. This method is then used to examine how different polyhedrons react to line and point displacements applied to their edges and corners. The described feature of being able to handle displacements and forces on edges and corners can improve modeling approaches in cases where highly localized stresses and strains occur, as in the studies by de Oliveira Góes et al. (2014), Placidi (2015, 2016), and Yang and Misra (2010, 2012).

For isotropic materials, Mindlin's theory of first-strain gradient elasticity (Mindlin 1965) is characterized by five material parameters in addition to two Lamé's parameters. In the literature, simplified versions of such a theory were proposed and used for dislocation modeling. For example, the theory of second-strain gradient elasticity or the so-called gradient elasticity of bi-Helmholtz type, which involves two material length scale parameters as new material coefficients, is proposed for the regularization of classical singularities and singularities of the hyperstresses as mentioned in Lazar et al. (2006). Indeed, one conclusion of Lazar et al. (2006) was that all relevant state quantities up to triple stresses can be regularized using gradient elasticity of bi-Helmholtz type. The regularization result produced by the use of higher-gradient models are presented and discussed by Lazar and Maugin (2006) concerning dislocations. In this case, the presence of higher gradients not only has a smoothing effect on the kinematical descriptors, but deeply modifies the mathematical nature of the displacement, keeping it as an ordinary monodromic functions also in cases in which this is not possible within Cauchy elasticity. Following Lazar et al. (2006), the regularization of the disclination fields was carried out by Deng et al. (2007). The application of gradient elasticity of bi-Helmholtz type for dislocation-based fracture mechanics was done by Mousavi (2016a, b). Furthermore, Shodja et al. (2012) determined all 15 gradient parameters plus the 4 characteristic length scales of Mindlin's isotropic second-strain gradient elasticity for some characteristic materials. In the cases examined by Shodja et al. (2012), all four characteristic length scales are in the range of Angstrom. The recent note by Polizzotto (2016) is also relevant as it provided a physical meaning of double and triple stresses and discussed some simple illustrative examples.

[1]Institut für Mechanik, Otto-von-Guericke-Univ., Universitätsplatz 2, 39106 Magdeburg, Germany.

[2]Dept. of Structural and Geotechnical Engineering, Univ. di Roma La Sapienza, 00185 Rome, Italy (corresponding author). E-mail: ivan.giorgio@uniroma1.it

[3]Professor, Institut für Mechanik, Otto-von-Guericke-Univ., Universitätsplatz 2, 39106 Magdeburg, Germany.

Note. This manuscript was submitted on April 29, 2016; approved on August 24, 2016; published online on October 28, 2016. Discussion period open until March 28, 2017; separate discussions must be submitted for individual papers. This paper is part of the ***Journal of Engineering Mechanics***, © ASCE, ISSN 0733-9399.

In the present paper, a particularly simple form for the dependence of the energy on second and third gradients of the displacement is chosen. The aim is to select the simplest possible object (deformation measure) fulfilling necessary objectivity requirements, whence the tensor norm. Since the main aim of the paper is to show regularization effects of higher-order dependence of the energy density when concentrated stresses are involved, any other choice seems to be unnecessarily complicated. A possible physical interpretation can follow from looking at the simplest monodimensional case. In this case, in the linear approximation, the energy density would simply depend on the square of (1) the slope, (2) the curvature, and (3) the spatial variation of the curvature, which corresponds to a generalized Hooke elastic model. The tensor norm of the second and third gradients of the displacement provides an average over all possible directions of the generalized Hooke elasticity displayed by the material.

Many materials, although showing considerable complexity in their structure and interior architecture, can be modeled at a small length scale by a classical Cauchy medium. Such a model can be characterized by a very large number of degrees of freedom even for a small sample. This choice, on the one hand, allows use of standard numerical tools based on finite-element methods, which are optimized for this kind of model. On the other hand, the complexity of the considered continua makes the use of such a model unsuitable from the point of view of computational costs. In this context, the use of higher-gradient models allows one to obtain a sufficiently accurate solution (e.g., Andreaus et al. 2016; Pideri and Seppecher 1997; Alibert and Della Corte 2015; Seppecher et al. 2011), completely comparable with the one from Cauchy theory, but by means of much smaller computational costs. In the literature, indeed, there are many examples of complex materials, the continuum models of which are obtained by a homogenization procedure that leads to micromorphic generalized continua, and, as a particular case, higher-gradient continua [e.g., Dos Reis and Ganghoffer (2012), Eremeyev (2005), Federico and Grillo (2012), and AminPour and Rizzi (2016) for generalized continua with microstructure and Turco et al. (2016), dell'Isola et al. (2016a, b), Scerrato et al. (2016a, b), and Challamel et al. (2015) for higher-gradient continua]. The use of higher-gradient models involves the increase of material parameters necessary to describe the more-detailed characterization of deformations of the material under study. For this reason, specific tests, both experimental and numerical, may be designed to identify such parameters as proposed by Placidi et al. (2015, 2016), Lekszycki et al. (1992), and Carrella and Ewins (2011) for dynamic properties as dissipation coefficients or parameters related to frequency-response functions. Moreover, in many particle systems, the analysis of dissipation phenomena involves a homogenization to describe finite dimensional systems in which length and time scales may be significant by means of a higher-gradient continuum approximation. Carcaterra et al. (2006), for instance, proposed a homogenization in a stochastic system and a perturbation analysis using a special family of probability distributions. The obtained continuum models are characterized by elastic and dissipative constitutive equations in which memory effects appear.

The present work is organized as follows. In section "Mathematical Formulation of the Problem," an elastic energy, $\mathcal{W}$, is introduced, that depends on the first, second, and third gradient of the displacement field $\mathbf{u}$. From the first variation of $\mathcal{W}$, generalized stress tensors are derived as well as the boundary conditions. This provides an understanding of why a third-gradient material can sustain point and line forces at corners and edges, a second-gradient material can sustain line forces at edges, and a classic Cauchy continuum can only sustain surface forces. In section "Implementation in a FEM Software," the implementation of a third-gradient and second-gradient material in the finite-element method (FEM) software package *COMSOL Multiphysics* is explained. Lagrangian multipliers are used to tie auxiliary tensors $\mathbf{Q}$ and $\mathbf{K}$ to the first and second gradient of $\mathbf{u}$, respectively. This is necessary since the first four derivatives of the displacement field $\mathbf{u}$ are involved, but only the first two derivatives of a tensor field can be obtained numerically without problems. In section "Tetrahedron," this FEM model is applied to examine a tetrahedron where the bottom surface is fixed and a displacement is prescribed at the tip point. Then, the case of a fixed bottom surface and a prescribed edge displacement is examined. Similarly, in section "Cube," a cube with prescribed corner or edge displacements is examined.

Mathematical Formulation of the Problem

In this section, the notation and formalism from Javili et al. (2013) is adopted. Slight modifications of the notation will be pointed out. A (small) elastic deformation of a hyperelastic material is described by the displacement field $\mathbf{u}$ on a three-dimensional (3D) body $\mathcal{B}$:

- $\partial\mathcal{B}$ denotes the boundary of $\mathcal{B}$, where $\partial\mathcal{B}$ is assumed as a finite, continuous union of bounded smooth surfaces;
- $\partial^2\mathcal{B}$ denotes the union of all edges of $\mathcal{B}$. Thus $\partial^2\mathcal{B}$ is defined as the (finite) union of the boundaries of the surfaces that build $\partial\mathcal{B}$; and
- $\partial^3\mathcal{B}$ denotes the union of all vertices of $\mathcal{B}$. Therefore $\partial^3\mathcal{B}$ is defined as the union of all the start and end points of the edges.

Furthermore, the tensor $\mathbf{E} := 1/2[\text{grad}(\mathbf{u}) + \text{grad}^T(\mathbf{u})]$ is the strain tensor. The elastic energy is defined as a functional

$$\mathcal{W} = \int_{\mathcal{B}} w[\mathbf{E}, \text{grad}^2(\mathbf{u}), \text{grad}^3(\mathbf{u})]dv \tag{1}$$

With $\delta\mathbf{E} = \text{grad}(\delta\mathbf{u})$, the first variation of $\mathcal{W}$ takes the form

$$\delta\mathcal{W} = \int_{\mathcal{B}} \mathbf{P}_1{:}\delta\mathbf{E} + \mathbf{P}_2 \ \cdots \ \text{grad}^2(\delta\mathbf{u}) + \mathbf{P}_3{::}\text{grad}^3(\delta\mathbf{u}) \tag{2}$$

where grad^2 and grad^3 = second and third gradient, respectively. A contraction of order two, three, or four is denoted by (1) a colon (:), (2) ellipses (⋯), or (3) a double colon (::), respectively. The tensors $\mathbf{P}_1$, $\mathbf{P}_2$, and $\mathbf{P}_3$ are Cauchy-type stresses, double stresses, and triple stresses, respectively. They are defined by

$$\mathbf{P}_1 := \frac{\partial w}{\partial \mathbf{E}} \tag{3}$$

$$\mathbf{P}_2 := \frac{\partial w}{\partial \text{grad}^2(\mathbf{u})} \tag{4}$$

$$\mathbf{P}_3 := \frac{\partial w}{\partial \text{grad}^3(\mathbf{u})} \tag{5}$$

In the context of the present work, only small deformations are considered. Therefore, there is no need to distinguish between a spatial and a reference placement. The following abbreviations will be used:

$\tilde{\mathbf{N}}$ denotes the normal vector on the smooth points of $\partial\mathcal{B}$ (6)

$\widetilde{\mathbf{N}}$ denotes the Frenet − Serret normal vector of a curve in $\partial^2\mathcal{B}$ (7)

$\hat{\mathbf{M}}$ denotes the projection of $\tilde{\mathbf{N}}$ onto the tangent plane of $\partial\mathcal{B}$ (8)

$\tilde{\mathbf{M}}$ denotes the Frenet − Serret binormal to $\partial^2\mathcal{B}$ (9)

$\hat{\kappa}_m$ denotes twice the mean curvature of smooth points in $\partial\mathcal{B}$ (10)

$\tilde{\kappa}_m$ denotes the curvature of curves in $\partial^2\mathcal{B}$ (11)

Furthermore, two operators have been defined. For a tensor $\mathbf{T}$

$$\hat{\mathbf{S}}(\mathbf{T}):\hat{\kappa}_m \cdot \hat{\mathbf{N}} + \widehat{\mathrm{div}}_{\parallel}(\mathbf{T}) \tag{12}$$

$$\tilde{\mathbf{S}}(\mathbf{T}):\tilde{\kappa}_m \cdot \tilde{\mathbf{N}} + \widetilde{\mathrm{div}}_{\parallel}(\mathbf{T}) \tag{13}$$

where the following definitions have been used:

$$\widehat{\mathrm{div}}_{\parallel}(\mathbf{T}):\mathrm{grad}(\mathbf{T}):\hat{\mathbf{Q}}_{\parallel} \qquad \text{(surface divergence)} \tag{14}$$

$$\widetilde{\mathrm{div}}_{\parallel}(\mathbf{T}):\mathrm{grad}(\mathbf{T}):\tilde{\mathbf{Q}}_{\parallel} \qquad \text{(curve divergence)} \tag{15}$$

where $\hat{\mathbf{Q}}_{\parallel}$ and $\tilde{\mathbf{Q}}_{\parallel}$ = projectors onto the surfaces in $\partial\mathcal{B}$ and the curves in $\partial^2\mathcal{B}$, respectively.

Following the lines of Mindlin (1965), Javili et al. (2013), or Bertram (2016b), the surface divergence theorem can be used to obtain

$$\begin{aligned}
\delta\mathcal{W} = &\int_{\mathcal{B}} [\mathrm{div}(\mathbf{P}_1) + \mathrm{div}^2(\mathbf{P}_2) + \mathrm{div}^3(\mathbf{P}_3)] \cdot \delta\mathbf{u} \\
&+ \int_{\partial\mathcal{B}} (\mathbf{P}_1 \cdot \hat{\mathbf{N}} - \mathrm{div}(\mathbf{P}_2) \cdot \hat{\mathbf{N}} - \hat{\mathbf{S}}(\mathbf{P}_2 \cdot \hat{\mathbf{N}}) + \mathrm{div}^2(\mathbf{P}_3) \\
&\cdot \hat{\mathbf{N}} - \hat{\mathbf{S}}(-\mathrm{div}(\mathbf{P}_3) \cdot \hat{\mathbf{N}}) - \hat{\mathbf{S}}([\mathbf{P}_3:[\hat{\mathbf{N}} \otimes \hat{\mathbf{N}}]]\hat{\kappa}_m) + \hat{\mathbf{S}}^2(\mathbf{P}_3 \cdot \hat{\mathbf{N}})) \cdot \delta\mathbf{u} \\
&+ \int_{\partial\mathcal{B}} (\mathbf{P}_2:[\hat{\mathbf{N}} \otimes \hat{\mathbf{N}}] - \mathrm{div}(\mathbf{P}_3):[\hat{\mathbf{N}} \otimes \hat{\mathbf{N}}] \\
&- \hat{\mathbf{S}}(\mathbf{P}_3:[\hat{\mathbf{N}} \otimes \hat{\mathbf{N}}]) - \hat{\mathbf{S}}(\mathbf{P}_3 \cdot \hat{\mathbf{N}}) \cdot \hat{\mathbf{N}}) \cdot \widehat{\mathrm{grad}}_N(\delta\mathbf{u}) \\
&+ \int_{\partial\mathcal{B}} (\mathbf{P}_3 \cdots [\hat{\mathbf{N}} \otimes \hat{\mathbf{N}} \otimes \hat{\mathbf{N}}] \cdot \widehat{\mathrm{grad}}_N^2(\delta\mathbf{u}) \\
&+ \int_{\partial^2\mathcal{B}} \sum_{\xi} (\mathbf{P}_2:[\hat{\mathbf{M}} \otimes \hat{\mathbf{N}}] + \mathrm{div}(\mathbf{P}_3):[\hat{\mathbf{M}} \otimes \hat{\mathbf{N}}] \\
&+ [\mathbf{P}_3:[\hat{\mathbf{N}} \otimes \hat{\mathbf{N}}]\hat{\kappa}_m \cdot \hat{\mathbf{M}} - \hat{\mathbf{S}}(\mathbf{P}_3 \cdot \hat{\mathbf{N}}) \cdot \hat{\mathbf{M}} - \tilde{\mathbf{S}}(\mathbf{P}_3:[\hat{\mathbf{M}} \otimes \hat{\mathbf{N}}])) \cdot \delta\mathbf{u} \\
&+ \int_{\partial^2\mathcal{B}} \sum_{\xi} (\mathbf{P}_3 \cdots [\hat{\mathbf{M}} \otimes \hat{\mathbf{N}} \otimes \hat{\mathbf{N}}]) \cdot \widehat{\mathrm{grad}}_N(\delta\mathbf{u}) \\
&+ \int_{\partial^2\mathcal{B}} \sum_{\xi} (\mathbf{P}_3 \cdots [\tilde{\mathbf{N}} \otimes \hat{\mathbf{M}} \otimes \hat{\mathbf{N}}]) \cdot \widetilde{\mathrm{grad}}_N(\delta\mathbf{u}) \\
&+ \int_{\partial^2\mathcal{B}} \sum_{\xi} (\mathbf{P}_3 \cdots [\tilde{\mathbf{M}} \otimes \hat{\mathbf{M}} \otimes \hat{\mathbf{N}}]) \cdot \widetilde{\mathrm{grad}}_M(\delta\mathbf{u}) \\
&+ \int_{\partial^3\mathcal{B}} \sum_{\mu,\xi} (\mathbf{P}_3 \cdots [\tilde{\mathbf{T}} \otimes \hat{\mathbf{M}} \otimes \hat{\mathbf{N}}]) \cdot \delta\mathbf{u}
\end{aligned} \tag{16}$$

The indices μ and ξ index the vertices and edges, respectively. The formula in Eq. (16) is derived by Javili et al. (2013) in great detail, and the notation therein is almost exactly adopted here to facilitate comparisons. Bertram (2016b) further reduced some surface terms. For the present work, the form in Eq. (16) is fully sufficient, since the higher-order traction terms, which are contracted with the normal gradients of $\delta\mathbf{u}$ in Eq. (16), are set to zero on the boundary in the examined cases.

Eq. (16) has two important implications, which have been pointed out (Javili et al. 2013):

- A body must be equipped at least with a second-gradient elastic energy to sustain concentrated line tractions at its edges; and
- A body must be equipped at least with a third-gradient elastic energy to sustain concentrated point tractions at its vertices.

Both are consequences of the fact that on the right-hand side of Eq. (16), the terms on the edges and vertices are balanced by gradient terms on the right-hand side. These observations will be substantiated in this work. Lazar et al. (2006) described a similar finding for the case of dislocations in two dimensions.

Implementation in a FEM Software

As explained in section "Mathematical Formulation of the Problem," the elastic energy must depend at least on $\mathrm{grad}^2(\mathbf{u})$ for the bulk to sustain line forces or displacements. It must depend at least on $\mathrm{grad}^3(\mathbf{u})$ for the bulk to sustain line and point forces or displacements at corners and edges. Since standard finite-element methods are optimized for first-gradient continua in numerical integration codes, derivatives of orders greater than one should be avoided. For this reason, in order to employ a standard finite-element (FE) environment, a Hellinger-Reissner type variational principle is used, which leads the numerical problem back to a more-comfortable standard formulation suitable for first-gradient continua (e.g., Dimitrijevic and Hackl 2008; Peerlings et al. 2004). The key idea here is to introduce more kinematical fields and Lagrange multipliers, which enable the writing of a potential energy of the first-gradient equivalent to that of the problem under study. In this way, even if the number of the kinematical descriptors increases, it is possible to use lower-order interpolation polynomials, which are suited for numerical classical problems. In detail, micromorphic tensors are introduced in the FE code

$$\mathbf{K}, \text{ which is constrained to be grad } \mathbf{u} \text{ and} \tag{17}$$

$$\mathbf{Q}, \text{ which is constrained to be grad } \mathbf{K} \tag{18}$$

as well as micromorphic constraints, which are introduced by using Lagrange multipliers $\mathbf{\Lambda_1}$ and $\mathbf{\Lambda_2}$ (both are tensors).

The rendering of a higher-gradient model by means of a microstructured continuum with Lagrange multipliers is a standard numerical technique that relies on the fact that the two models in the bulk are equivalent. In this regard, it has to be pointed out that there is no general proof that the two models will coincide concerning the boundary conditions. However, in some particular cases, the equivalence has indeed been proven. Bleustein (1967) established the relationship between the boundary conditions of the Mindlin microstructure theory and of the linearized Toupin strain gradient theory, assuming a componentwise convergence of the tensorial microstructural descriptor to the gradient of the displacement, whence a clear physical interpretation for the external forces in the strain-gradient theory is provided. The microstructural tensor descriptors and the displacement cannot be varied arbitrarily because of the coupling implied by the Lagrange multipliers. This means that the variation of the microstructure terms on the boundary will be coupled with the variation of the displacement. From a physical point of view, this is the origin of edge and corner contributions in the microstructured case. A complete mathematical treatment of this problem will be worthy of further investigation. Another problem for a general equivalence theorem is linked to the fact that the integration by parts leading to the strong formulation of the problem requires suitable regularity assumptions on

the Lagrange multipliers [see for instance Duistermaat and Kolk's (2004) corollary 7.6.2]. A reasonably general proof of the equivalence of the boundary conditions in the two cases would also require the proof that the generalized stresses represented by Λ_1 and Λ_2 always fulfill these regularity assumptions, at least for some classes of boundary conditions. This is indeed a delicate point that will be addressed in future investigations. In the present paper, however, only boundary conditions concerning simple displacements applied on edges and corners are considered, because one may expect not to produce pathological solutions.

The third-gradient elastic energy for the variables $\mathbf{E}$, $\mathbf{K}$, and $\mathbf{Q}$, and under the assumption of isotropic and homogenous material, is assumed to be

$$W_{\text{grad}^3}(\mathbf{E},\mathbf{K},\mathbf{Q}) := \underbrace{\frac{1}{2}[2\mu\mathbf{E}:\mathbf{E}+\lambda tr(\mathbf{E})^2]}_{=W_{\text{I}}(\mathbf{E})} + \underbrace{\frac{1}{2}\lambda_1 \text{grad}\mathbf{K} \cdots \text{grad}\mathbf{K}}_{=W_{\text{II}}(\mathbf{K})} + \underbrace{\frac{1}{2}\lambda_2 \text{grad}\mathbf{Q}::\text{grad}\mathbf{Q}}_{=W_{\text{III}}(\mathbf{Q})} + \boldsymbol{\Lambda}_1:(\mathbf{K}-\text{grad}\mathbf{u}) + \boldsymbol{\Lambda}_2 \cdots (\mathbf{Q}-\text{grad}\mathbf{K}) \tag{19}$$

where λ and μ = Lamé parameters; and λ_1 and λ_2 = second-gradient and third-gradient stiffnesses, respectively.

The second-gradient elastic energy for the variables $\mathbf{E}$ and $\mathbf{K}$ is specified as

$$W_{\text{grad}^2}(\mathbf{E},\mathbf{K}) := W_{\text{I}}(\mathbf{E}) + W_{\text{II}}(\mathbf{K}) + \boldsymbol{\Lambda}_1 \cdots (\mathbf{K}-\text{grad}\mathbf{u}) \tag{20}$$

The energies have been brought into a dimensionless form by choosing a reference length scale l_{ref} and a reference Lamé constant λ_{ref}. This means that the real material constants are related to the reference constants

$$\lambda = \frac{\lambda_{\text{real}}}{\lambda_{\text{ref}}}, \qquad \mu = \frac{\mu_{\text{real}}}{\lambda_{\text{ref}}}, \qquad \lambda_1 = \frac{\lambda_{1_{\text{real}}}}{\lambda_{\text{ref}} l_{\text{ref}}^2}, \qquad \lambda_2 = \frac{\lambda_{2_{\text{real}}}}{\lambda_{\text{ref}} l_{\text{ref}}^4} \tag{21}$$

The problem of solving the boundary value problem of a second-gradient or third-gradient material now reduces to the variational problem of finding an extremum of W_{grad^3} or W_{grad^2} on a certain set of shape functions subject to constraints. For all simulations, $\lambda = 1$ and $\mu = 0.08$ have been set. Except for the section "Parameter Study for λ_1 and λ_2" with the parameter study on λ_1 and λ_2, the values $\lambda_1 = 0.04$ and $\lambda_2 = 0.0015$ have been set. In this paper, rather than addressing the description of materials existing in nature presenting noticeable scale-effects, the authors propose higher-gradient models as a tool for the mathematical description of objects manufactured by means of computer-assisted methods (3D printing, electrospinning etc.). These mechanical systems can show (and exploit) scale effects corresponding to a wide class of possible length scales (dell'Isola et al. 2015c). For instance, truss modular beams and pantographic structures can have periodic cells of some microns when the total length of the sample is of the order of centimeters, or periodic cells of some centimeters when the total length is of the order of meters, and so on. Therefore, the choice for the coefficients here proposed is exemplary and does not exclude other possible choices. Indeed, it ensures that the gradient effects occur in a boundary layer of size $\ell = 0.2 l_{\text{ref}}$, which can be captured by the meshes that have been used.

The software package *COMSOL Multiphysics* has been used to implement the approach described beforehand. This is done by using the weak-form feature of the software that allows the user to enter the variational problem directly. The software solves for the fields u_i, K_{ij}, and Q_{ijk} and the Lagrange multipliers $\Lambda_{1_{ij}}$ and $\Lambda_{2_{ijk}}$ in the third-gradient cases or for the fields u_i, K_{ij}, and the Lagrange multiplier $\Lambda_{1_{ij}}$ in the second-gradient cases. The software solves $\delta W_{\text{grad}^3} = 0$ or $\delta W_{\text{grad}^2} = 0$ with $\mathbf{E}$, $\mathbf{K}$, $\mathbf{Q}$, $\boldsymbol{\Lambda}_1$, and $\boldsymbol{\Lambda}_2$ being cubic Lagrange shape functions. Further Lagrange multipliers are needed to implement displacement boundary conditions. These multipliers are chosen to be quadratic Lagrange shape functions in order to be consistent with the aforementioned assumptions. By using an expedient formulation in the present work, the capabilities of the considered constitutive relations in Eqs. (19) and (20) are investigated, but for future developments, more-specific numerical tools could be considered, such as those implemented by Fischer et al. (2010), Greco and Cuomo (2016), and Cazzani et al. (2016). In the following sections, the deformation for several polyhedrons equipped with the introduced gradient energy is presented. The grayscale in all figures represents the stored elastic energy.

Tetrahedron

The tetrahedron has been chosen for extensive numerical studies, since it is the simplest polyhedron to demonstrate the effect of the second-strain gradient in the elastic energy.

Tetrahedron with One Point Displacement and One Fixed Surface

A tetrahedron with each side of length l_{ref} is subjected to a displacement of magnitude $0.05 l_{\text{ref}}$ at the tip to satisfy the small deformation assumption. The displacement vector is orthogonal to the surface opposite to the vertex to which the displacement is applied. In Fig. 1, one can see that for the classic first-gradient energy the displacement field and the elastic energy both are mesh-dependent. The displacement field and energy clearly tend to a solution with a singularity at the tip. This is apparent from the fact that the induced displacement and energy for any mesh are concentrated in the cell at the tip and vanish everywhere else. The energy density grows unbounded, as can be seen on the scale bar on the right of the bodies. The solutions for the second-gradient energy in Fig. 2 show a less-pronounced mesh-dependence. In contrast to the case with a first-order energy, the displacement field does not show any indication of mesh-dependence. However, the second-gradient energy is clearly mesh-dependent, which is again apparent from the facts that it is confined to the finite element at the tip, and that its density maximum grows with each mesh refinement. It can therefore be concluded that the solutions tend to a limit where the displacement is continuous but the second-gradient energy has a singularity at the tip. Only the solution for a third-gradient energy in Fig. 3 can be regarded as mesh-independent since both the elastic energy and the displacement undergo negligible changes when the mesh is refined.

In Fig. 4, the energy density at the tip is plotted as a function of the representative mesh size in the neighborhood of the displaced corner for the three examined cases, i.e., first-gradient, second-gradient, and third-gradient elastic energy models. A numerical evaluation of the absolute value of the right derivative at the smallest considered mesh size provides, respectively, 34,957.9, 101,608.9, and 0.032 for first-gradient, second-gradient, and third-gradient elastic energy models. It is clear from these values that only the numerical solution of the third-gradient elastic model is reliable when such kinds of boundary conditions at the tip are applied.

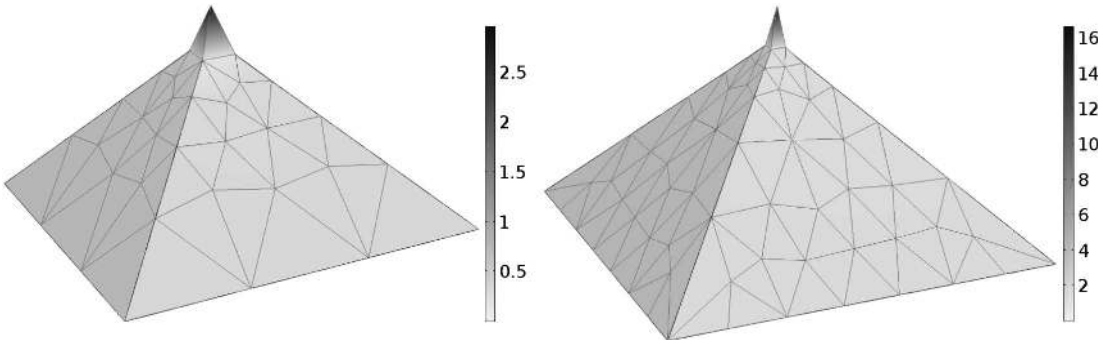

Fig. 1. Mesh-dependent solution for tip displacement with first-order elastic energy

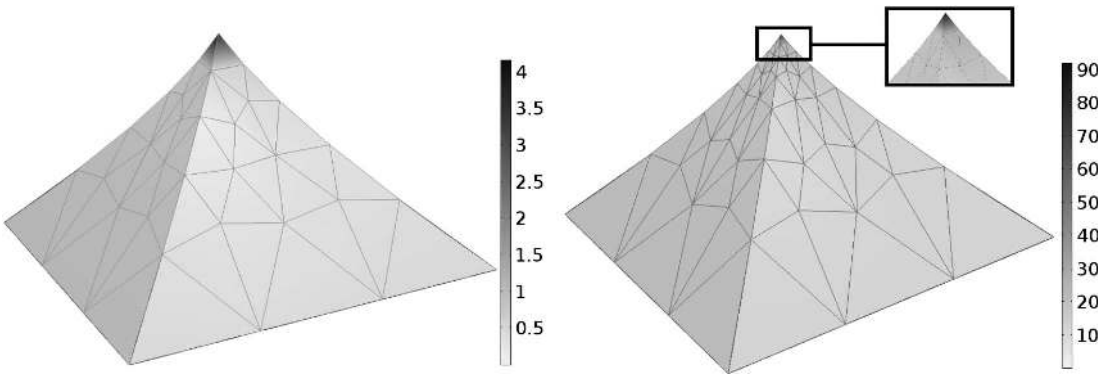

Fig. 2. Mesh-dependent solution for tip displacement with second-gradient elastic energy

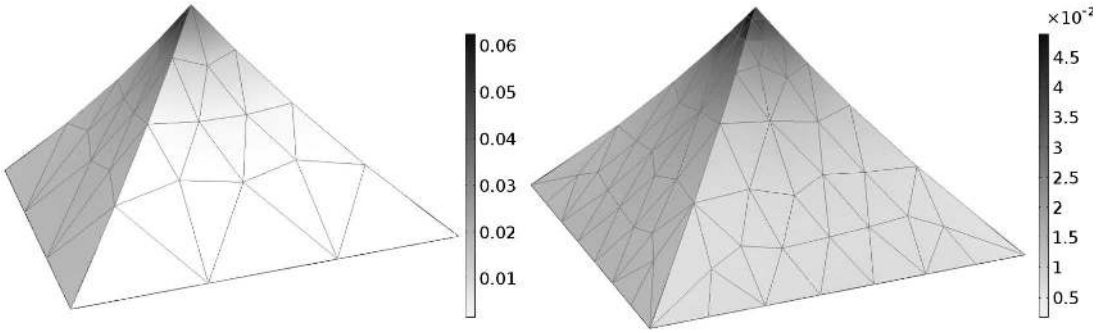

Fig. 3. Mesh-independent solution for tip displacement with third-gradient elastic energy

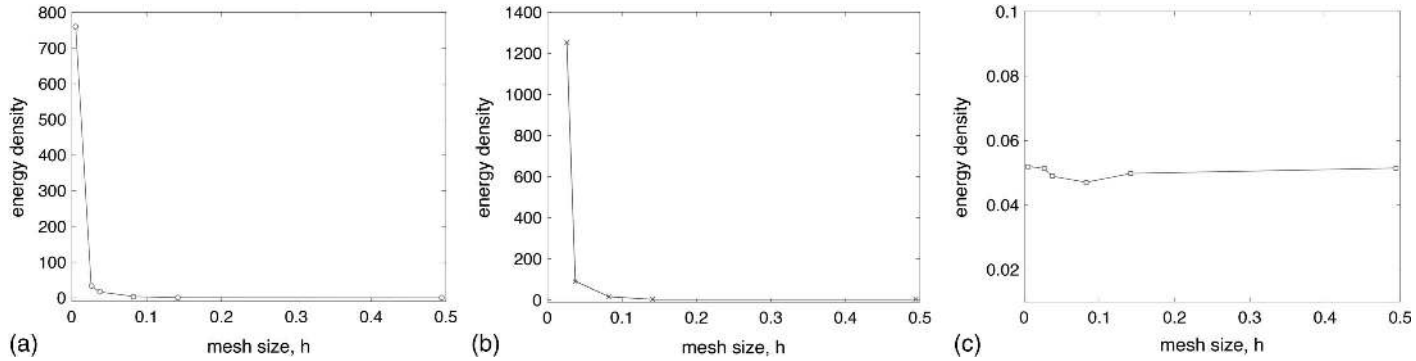

Fig. 4. Energy density versus mesh size at the tip of the tetrahedron for first-gradient, second-gradient, and third-gradient elastic energy models, respectively

Mesh Refinement Study for Third-Gradient Energy

A mesh refinement study has been conducted for the case of a third-gradient energy by applying several tetrahedral meshes. Refinement has mainly been concentrated on the tip where the displacement is prescribed, as shown in Fig. 5. In Fig. 6, one can see that the values for the components of the elastic energy vary in a small range as the mesh is refined. These results suggest that a mesh with a number of elements that lies in the middle of the evaluated range is sufficient for further numerical studies.

Fig. 7 shows an illustrative example where the distribution of the magnitude of the component u_1 of the displacement along one edge of the tetrahedron for the cases of (1) first-gradient and (2) third-gradient models for different values of the mesh size. The results show that, in the first case, the effect of the imposed displacement is concentrated in the last available mesh element, which is a typical numerical evidence of mesh-dependency. In contrast, the third-gradient model shows a perfectly sensible convergence to a reasonable solution.

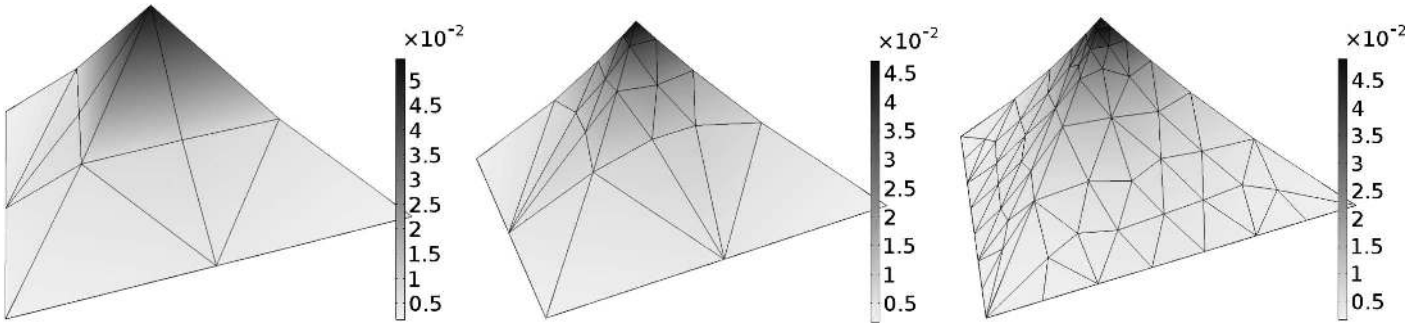

Fig. 5. Third-gradient energy: solutions for meshes with 46, 176, and 340 elements

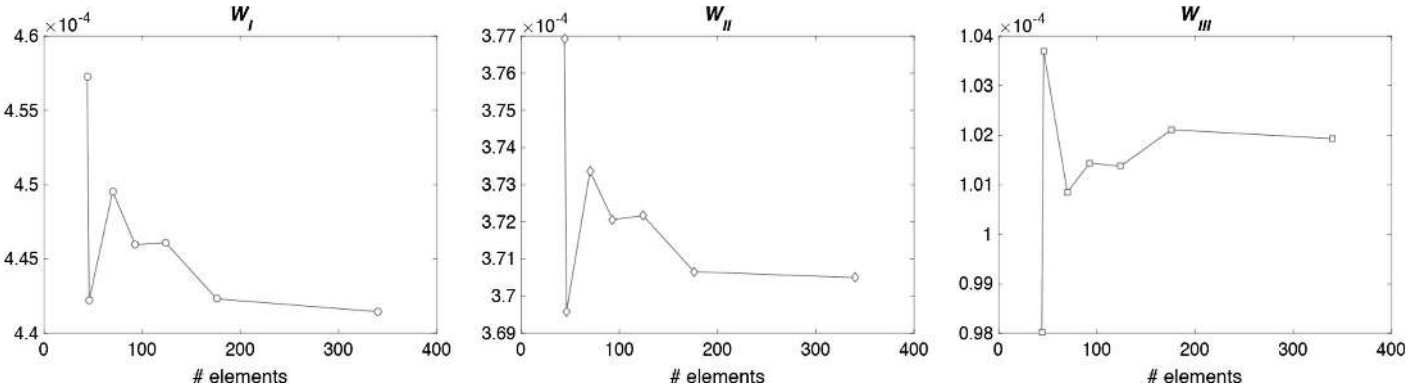

Fig. 6. Value of the components W_{I}, W_{II}, and W_{III} of the stored elastic third-gradient energy W_{grad^3} for meshes with different number of elements

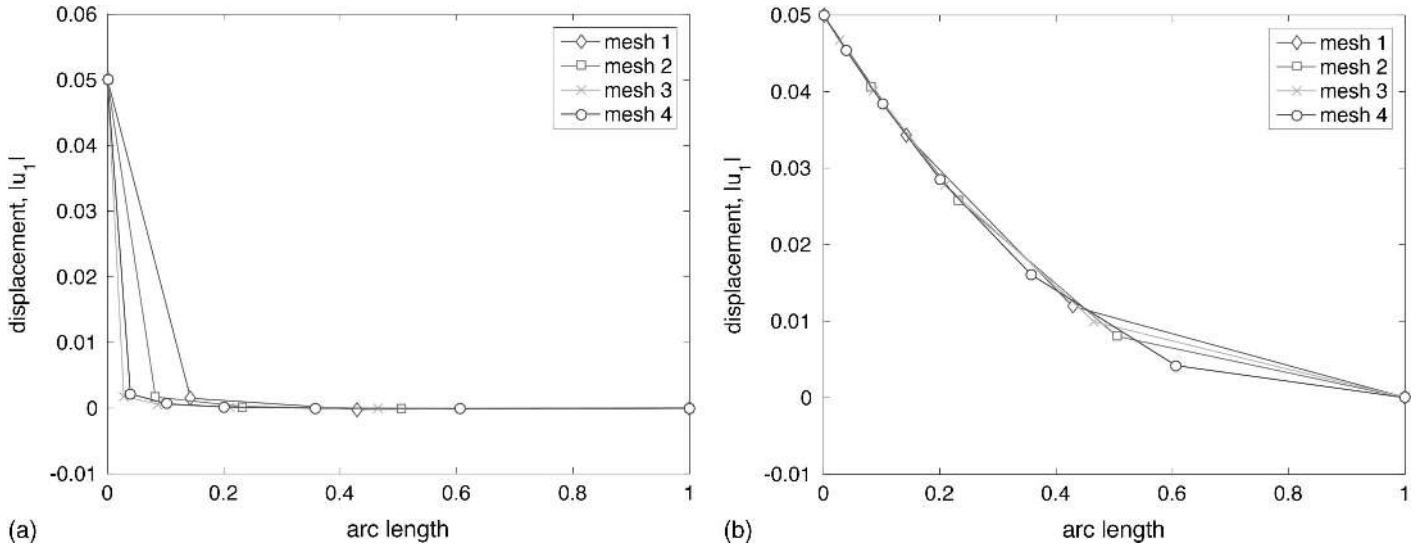

Fig. 7. Value of the amplitudes of the displacement component $|u_1|$ in the case of (a) first-gradient energy; (b) third-gradient energy W_{grad^3}, for meshes with different number of elements

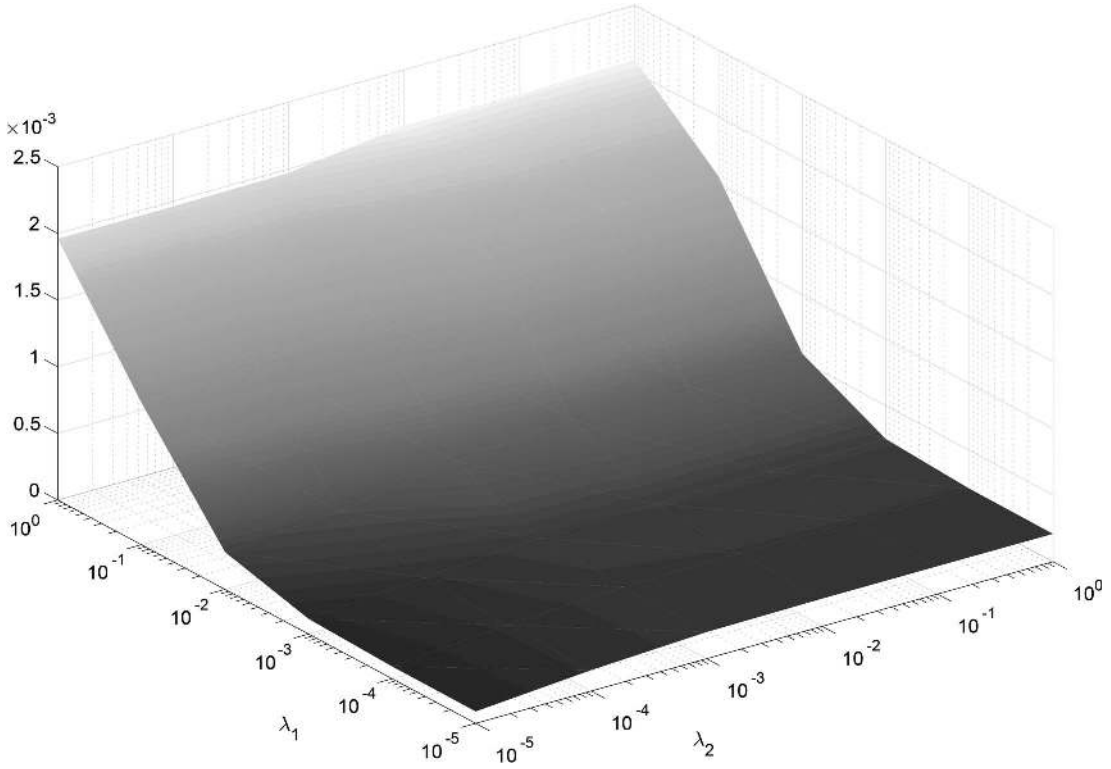

Fig. 8. Stored elastic third-gradient energy W_{grad^3} plotted over different ranges of λ_1 and λ_2

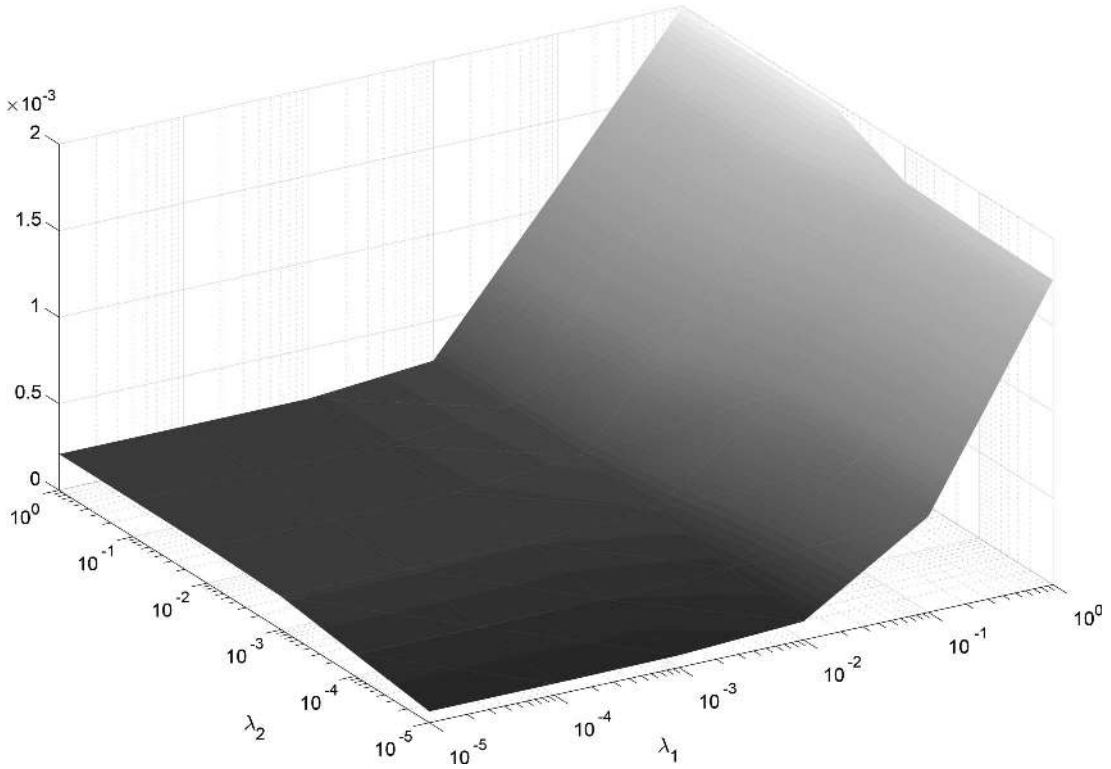

Fig. 9. Stored energy component W_I plotted over different ranges of λ_1 and λ_2

Parameter Study for λ_1 and λ_2

In order to understand the dependence of the third-gradient energy on the choice of the dimensionless material parameters λ, λ_1, and λ_2, a parameter study has been set up with $\lambda = 1$ and $\mu = 0.08$, as already mentioned. In Figs. 8–11, the dependence of the third-gradient energy W_{grad^3} and of its three components (W_I, W_{II}, and W_{III}) on the parameters λ_1 and λ_2 is visualized. The plots show that in this case, λ_1 has a greater influence on W_{grad^3} than λ_2.

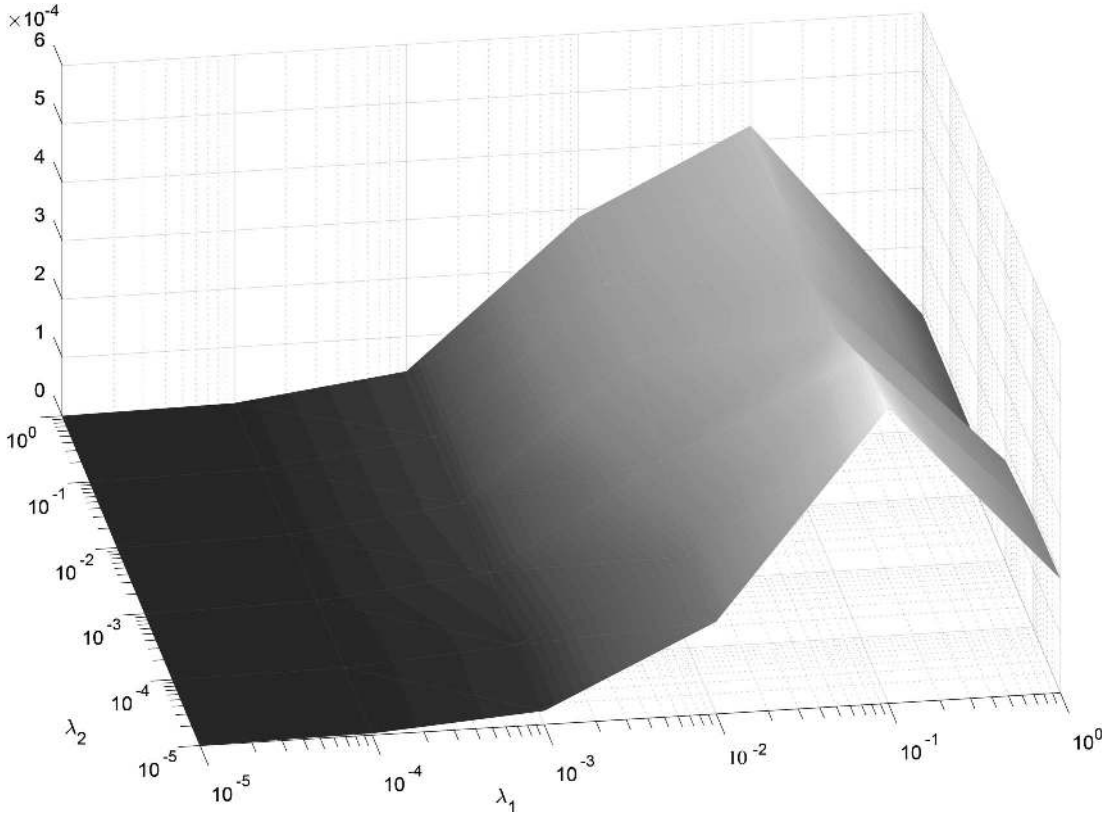

Fig. 10. Stored energy component W_{II} plotted over different ranges of λ_1 and λ_2

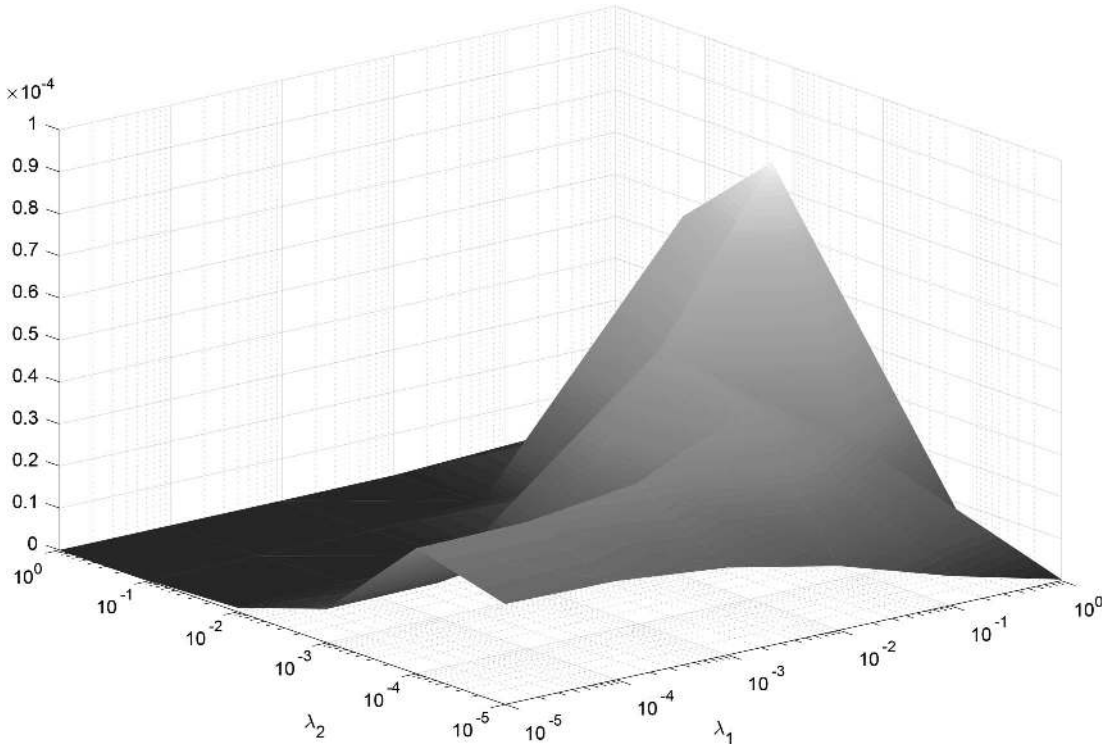

Fig. 11. Stored energy component W_{III} plotted over different ranges of λ_1 and λ_2

Tetrahedron with One Line Displacement and One Fixed Surface

The displacements are prescribed along one edge of the tetrahedron. The displacements increase linearly along the edge starting from zero at one point and reaching $0.05l_{ref}$ at the other point, as depicted in Fig. 12. The surface at the bottom is fixed. The solutions in Fig. 13 show that a first-gradient energy does not allow the bulk to sustain a line displacement. The solutions are clearly

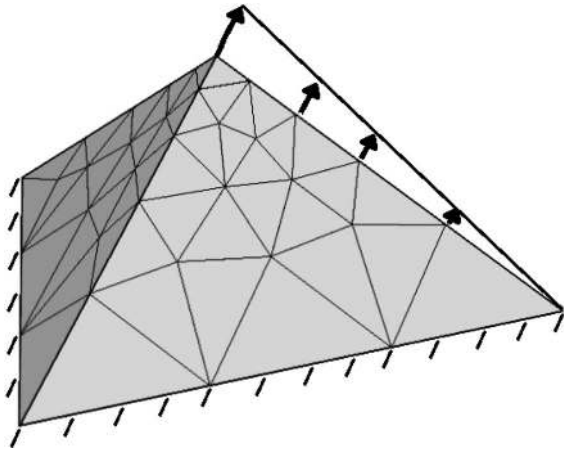

Fig. 12. Prescribed line displacement along an edge of a tetrahedron

mesh-dependent and tend to a line singularity, i.e., all points on the line with prescribed displacement become singularities. Fig. 14 shows that the solutions for a second-gradient material do not tend to a case with singularities in the displacement field. However, Fig. 14 gives evidence that the solutions tend to a case where the second-gradient energy has a singularity at the tip of the tetrahedron. Along the rest of the line, it appears that in the limit, the second-gradient energy assumes finite values. Of course, it could also be that in the limit, all points on the line become singularities of the second-gradient energy or that the second-gradient energy assumes finite values along the whole line, but with a discontinuity at the tip. In any case, it can be said that for the second-gradient energy, a line force results in a noncontinuous distribution of the second-gradient energy along the edge where a displacement is prescribed. The third-gradient energy in Fig. 15 clearly yields solutions that only vary to a small extent with variations of the mesh. This indicates mesh-independence, which means that no

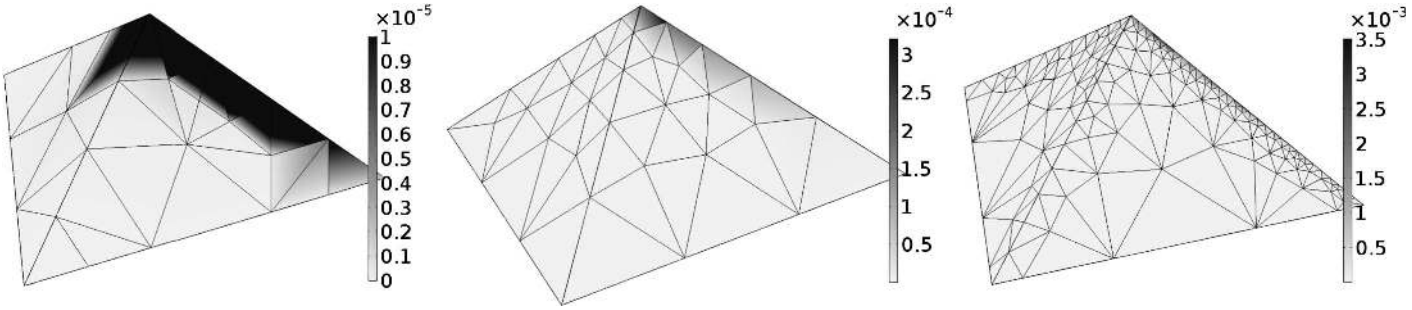

Fig. 13. Solution for a tetrahedron with prescribed nonconstant line displacement and fixed bottom surface equipped with the first-gradient energy (mapped in grayscale); the mesh becomes progressively finer around the edge with a prescribed line displacement

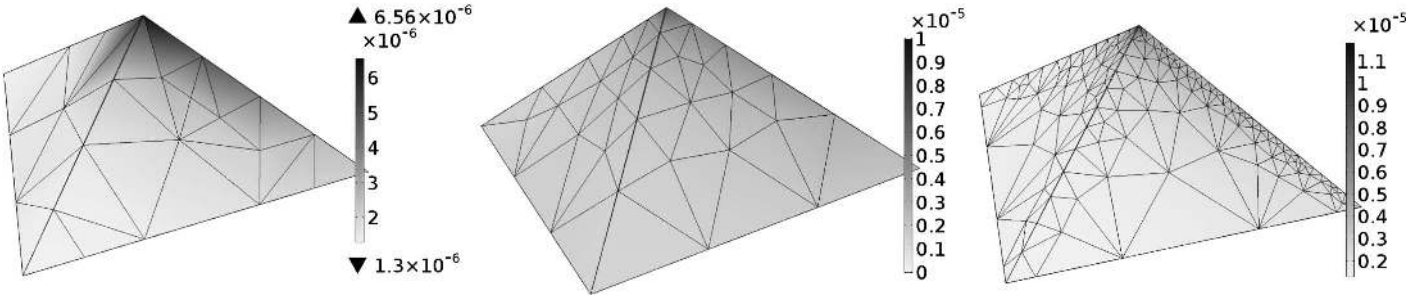

Fig. 14. Solution for a tetrahedron with prescribed nonconstant line displacement and fixed bottom surface equipped with the second-gradient energy (mapped in grayscale); the mesh becomes progressively finer around the edge with a prescribed line displacement

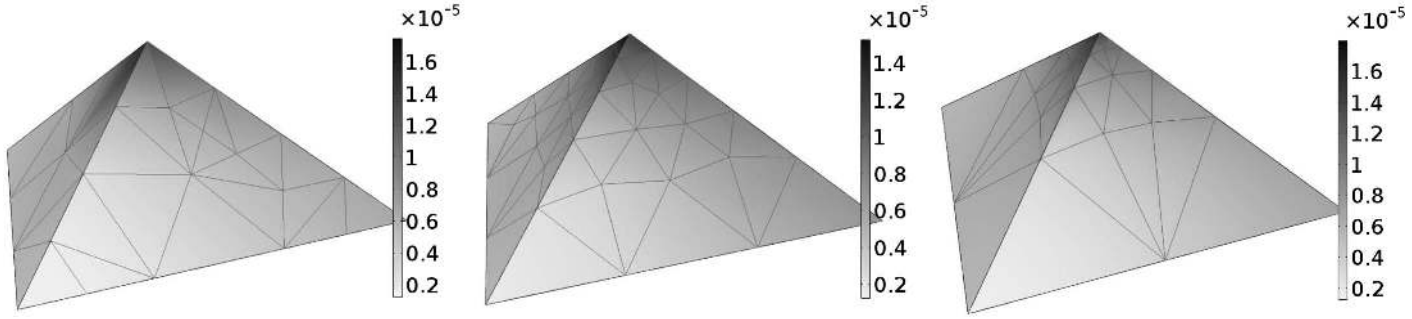

Fig. 15. Solution for a tetrahedron with prescribed nonconstant line displacement and fixed bottom surface equipped with the third-gradient energy (mapped in grayscale); the mesh becomes progressively finer around the edge with a prescribed line displacement

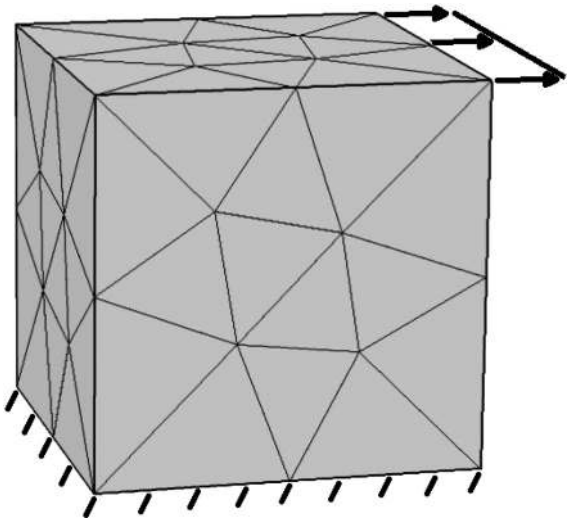

Fig. 16. Cube with fixed bottom surface and prescribed displacement at one edge

singularities in the displacement or the third-gradient energy are present. Therefore it confirms that a third-gradient energy allows the bulk to sustain line displacements. Comparing Figs. 14 and 15, the most noticeable difference is that in the second-gradient case, the energy is focused in a narrower region.

Figs. 13–15 show the solutions of the tetrahedron for the first-gradient, second-gradient, and third-gradient elastic energies with the prescribed line displacement from Fig. 12.

Cube

Cube with One Prescribed Shearlike Line Displacement and One Fixed Surface

A cube has been chosen to demonstrate the effect of a line displacement. The bottom of the cube has been fixed and a displacement of $0.5l_{\text{ref}}$ parallel to the bottom surface is prescribed as illustrated in Fig. 16.

For this geometry, the influence of the higher gradients is even more pronounced than for a tetrahedron. The solutions have similar properties as were already observed and explained in Figs. 13–15 in section "Tetrahedron." Fig. 17 shows that the classic first-gradient energy produces a solution that tends to a line singularity of the displacement field. The second-gradient material in Fig. 18 yields results that are similar to those obtained for the tetrahedron in Fig. 14. The displacement field is clearly continuous in the limit. In the limit, the second-gradient energy probably has finite values along the edge, with the prescribed displacement and singularities at its end points. The limit of the second-gradient energy could also have a discontinuity with finite values at the end points or a singularity along the whole edge. Fig. 19 shows that the third-gradient material can sustain the line displacement with no singularities in

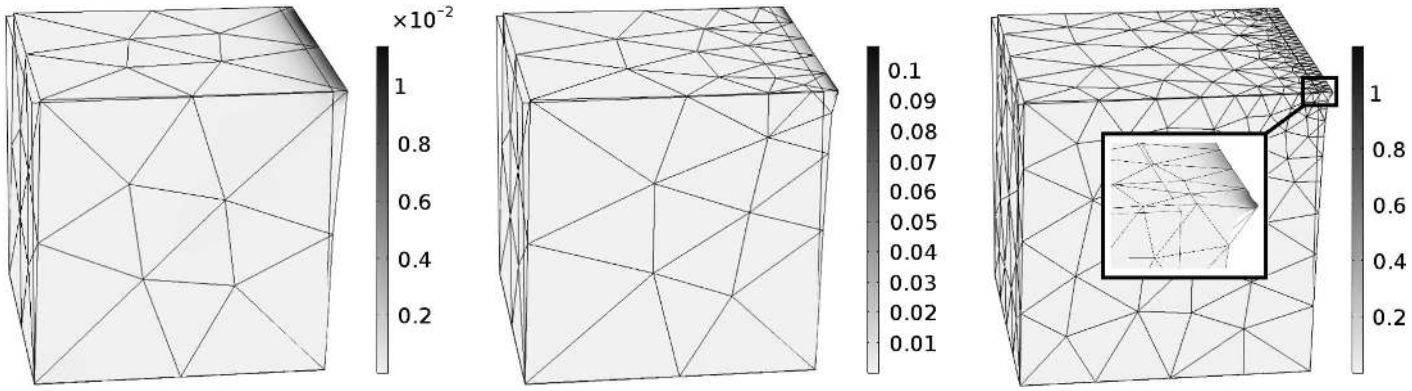

Fig. 17. Deformed cube with fixed bottom surface and prescribed displacement at one edge with the first-gradient energy; the mesh becomes progressively finer around the edge with a prescribed line displacement

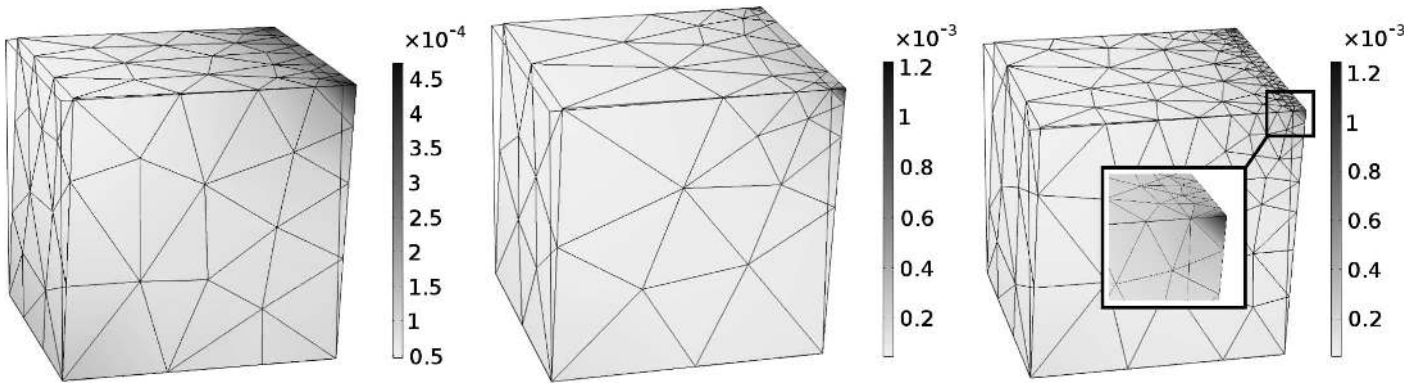

Fig. 18. Deformed cube with fixed bottom surface and prescribed displacement at one edge with the second-gradient energy; the mesh becomes progressively finer around the edge with a prescribed line displacement

the either displacement field or in the corresponding third-gradient elastic energy.

Cube with Point Displacements

Figs. 20 and 21 show two cases of prescribed corner displacements on a cube. In Fig. 20, a tip displacement has been applied in combination with a zero-displacement boundary condition at one surface of the cube. Displacement with magnitude $0.05l_{\text{ref}}$ is chosen in the direction of the space diagonal, while the fixed surface is in the x, y-plane. In Fig. 21, displacements of magnitude $0.05l_{\text{ref}}$ have been prescribed at four vertices; each displacement in direction of the space diagonal corresponds to the vertex where it is applied. In both cases, it is clear that a first-order material leads to a singularity in the displacement, and a second-order material results in continuous displacements with singularities in the gradient energy. The third-order material clearly yields a smooth solution with no singularities at all.

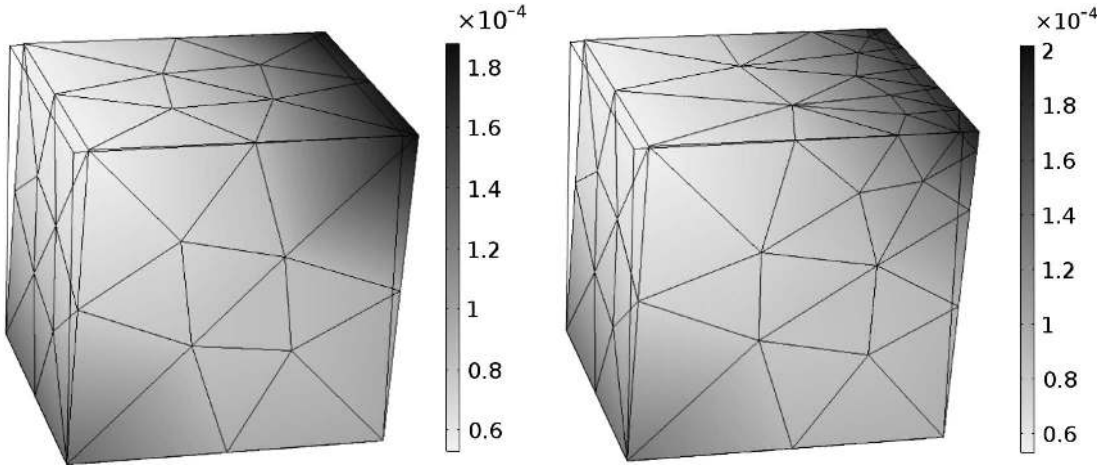

Fig. 19. Deformed cube with fixed bottom surface and prescribed displacement at one edge with the third-gradient energy; the mesh becomes progressively finer around the edge with a prescribed line displacement

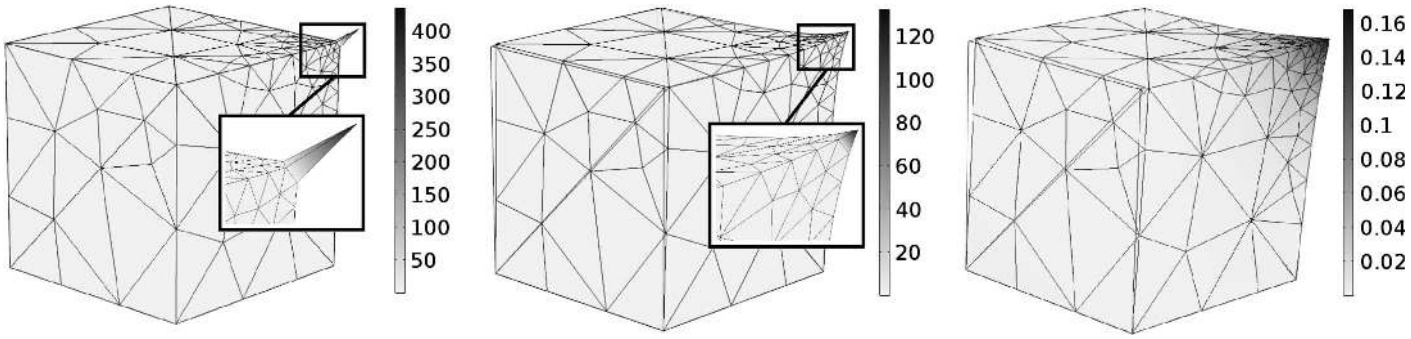

Fig. 20. Plot of the corresponding elastic energy for a first-order, second-order, and third-order material

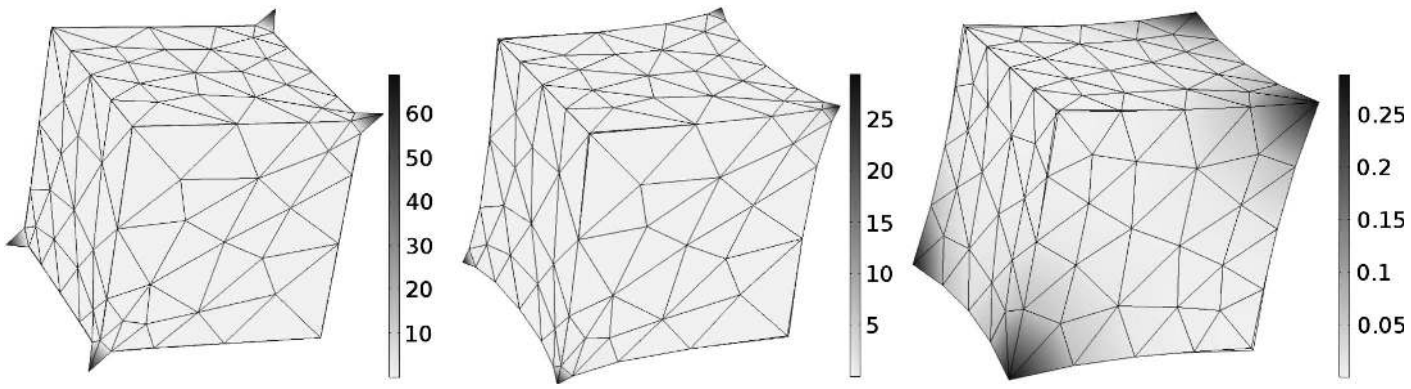

Fig. 21. Plot of the corresponding elastic energy for a first-order, second-order, and third-order material

Conclusions

In this paper, a numerical study was carried out concerning different polyhedra and with various boundary conditions for a material with a constitutive behavior described by the second and third gradient of the displacement. Such materials could be considered when a complex microstructure is present; indeed, a homogenization technique can lead to a target model of higher gradient [e.g., a microstructure that is related to a third-gradient continuum (Seppecher et al. 2011)]. From the presented numerical simulations, it is easy to consider that only third-gradient materials can sustain point forces at corners while first-gradient and second-gradient continua are not able do so. It has been shown that a second-gradient material under prescribed edge displacements yields a continuous solution for the displacement field with discontinuities or possibly even singularities at vertices. Moreover, because of the complex microstructure of the materials under consideration, issues related to loss of stability could be very relevant to investigate. One needs only think of loss of stability in porous materials such as metal and polymer foams or biological tissues as bone (e.g., Evdokymov et al. 2011). Specific tools as those presented by Pignataro et al. (2009), Gabriele et al. (2012), Rizzi and Varano (2011), Carassale and Piccardo (2010), and Challamel et al. (2015) can be profitably employed for this purpose.

Acknowledgments

The first author has been financially supported by Graduiertenkolleg 1554: Micro-Macro-Interactions in structured Media and Particle Systems of the DFG (German Science Foundation). Helpful comments and suggestions by Rainer Glüge are gratefully acknowledged.

References

Agiasofitou, E. K., and Lazar, M. (2009). "Conservation and balance laws in linear elasticity of grade three." *J. Elast.*, 94(1), 69–85.

Alibert, J.-J., and Della Corte, A. (2015). "Second-gradient continua as homogenized limit of pantographic microstructured plates: A rigorous proof." *Zeitschrift für angewandte Mathematik und Physik*, 66(5), 2855–2870.

Alibert, J.-J., Seppecher, P., and dell'Isola, F. (2003). "Truss modular beams with deformation energy depending on higher displacement gradients." *Math. Mech. Solids*, 8(1), 51–73.

AminPour, H., and Rizzi, N. (2016). "A one-dimensional continuum with microstructure for single-wall carbon nanotubes bifurcation analysis." *Math. Mech. Solids*, 21(2), 168–181.

Andreaus, U., dell'Isola, F., Giorgio, I., Placidi, L., Lekszycki, T., and Rizzi, N. L. (2016). "Numerical simulations of classical problems in two-dimensional (non) linear second gradient elasticity." *Int. J. Eng. Sci.*, 108, 34–50.

Bertram, A. (2015). "Finite gradient elasticity and plasticity: A constitutive mechanical framework." *Continuum Mech. Thermodyn.*, 27(6), 1039–1058.

Bertram, A. ed. (2016a). *Compendium on gradient materials*, 2nd Ed., Otto von Guericke Univ., Magdburg, Germany.

Bertram, A. (2016b). "Finite gradient elasticity and plasticity: A constitutive thermodynamical framework." *Continuum Mech. Thermodyn.*, 28(3), 869–883.

Bleustein, J. L. (1967). "A note on the boundary conditions of Toupin's strain-gradient theory." *Int. J. Solids Struct.*, 3(6), 1053–1057.

Carassale, L., and Piccardo, G. (2010). "Non-linear discrete models for the stochastic analysis of cables in turbulent wind." *Int. J. Non-Linear Mech.*, 45(3), 219–231.

Carcaterra, A., Akay, A., and Koc, I. M. (2006). "Near-irreversibility in a conservative linear structure with singularity points in its modal density." *J. Acoust. Soc. Am.*, 119(4), 2141–2149.

Carrella, A., and Ewins, D. (2011). "Identifying and quantifying structural nonlinearities in engineering applications from measured frequency response functions." *Mech. Syst. Signal Process.*, 25(3), 1011–1027.

Cazzani, A., Malagù, M., Turco, E., and Stochino, F. (2016). "Constitutive models for strongly curved beams in the frame of isogeometric analysis." *Math. Mech. Solids*, 21(2), 182–209.

Challamel, N., Kocsis, A., and Wang, C. M. (2015). "Higher-order gradient elasticity models applied to geometrically nonlinear discrete systems." *Theor. Appl. Mech.*, 42(4), 223–248.

Challamel, N., Zhang, Z., and Wang, C. M. (2015). "Nonlocal equivalent continua for buckling and vibration analyses of microstructured beams." *J. Nanomech. Micromech.*, 10.1061/(ASCE)NM.2153-5477.0000062, A4014004.

COMSOL Multiphysics version 5.2 [Computer software]. COMSOL AB, Stockholm, Sweden.

dell'Isola, F., Andreaus, U., and Placidi, L. (2015a). "At the origins and in the vanguard of peridynamics, non-local and higher-gradient continuum mechanics: An underestimated and still topical contribution of Gabrio Piola." *Math. Mech. Solids*, 20(8), 887–928.

dell'Isola, F., Della Corte, A., Greco, L., and Luongo, A. (2016a). "Plane bias extension test for a continuum with two inextensible families of fibers: A variational treatment with Lagrange multipliers and a perturbation solution." *Int. J. Solids Struct.*, 81, 1–12.

dell'Isola, F., Giorgio, I., Pawlikowski, M., and Rizzi, N. L. (2016b). "Large deformations of planar extensible beams and pantographic lattices: Heuristic homogenization, experimental and numerical examples of equilibrium." *Proc. R. Soc. A*, 472(2185), 20150790.

dell'Isola, F., Maier, G., Perego, U., Andreaus, U., Esposito, R., and Forest, S. (2014). "The complete works of Gabrio Piola: Volume I—Commented English translation." *Advanced structured materials*, Springer, Switzerland.

dell'Isola, F., Seppecher, P., and Della Corte, A. (2015c). "The postulations á la d'Alembert and á la Cauchy for higher gradient continuum theories are equivalent: A review of existing results." *Proc. R. Soc. London A*, 471(2183), 20150415.

dell'Isola, F., Steigmann, D., and Della Corte, A. (2015b). "Synthesis of fibrous complex structures: Designing microstructure to deliver targeted macroscale response." *Appl. Mech. Rev.*, 67(6), 060804.

Deng, S., Liu, J., and Liang, N. (2007). "Wedge and twist disclinations in second strain gradient elasticity." *Int. J. Solids Struct.*, 44(11), 3646–3665.

de Oliveira Góes, R. C., de Castro, J. T. P., and Martha, L. F. (2014). "3D effects around notch and crack tips." *Int. J. Fatigue*, 62, 159–170.

Dimitrijevic, B. J., and Hackl, K. (2008). "A method for gradient enhancement of continuum damage models." *Tech. Mech.*, 28(1), 43–52.

Dos Reis, F., and Ganghoffer, J. F. (2012). "Construction of micropolar continua from the asymptotic homogenization of beam lattices." *Comput. Struct.*, 112, 354–363.

Duistermaat, J. J., and Kolk, J. A. C. (2004). *Multidimensional real analysis II: Integration*, Cambridge University Press, New York.

Eremeyev, V. A. (2005). "Nonlinear micropolar shells: Theory and applications." *Shell structures: Theory and applications*, W. Pietraszkewicz and C. Szymczak, eds., Taylor & Francis, London, 11–18.

Evdokymov, N., Altenbach, H., and Eremeyev, V. A. (2011). "Collapse criteria of foam cells under various loading." *PAMM*, 11(1), 365–366.

Federico, S., and Grillo, A. (2012). "Elasticity and permeability of porous fibre-reinforced materials under large deformations." *Mech. Mater.*, 44, 58–71.

Fischer, P., Mergheim, J., and Steinmann, P. (2010). "On the C1 continuous discretization of non-linear gradient elasticity: A comparison of NEM and FEM based on Bernstein-Bézier patches." *Int. J. Numer. Methods Eng.*, 82(10), 1282–1307.

Gabriele, S., Rizzi, N., and Varano, V. (2012). "On the imperfection sensitivity of thin-walled frames." *Proc., 11 Int. Conf. on Computational Structures Technology*, B. H. V. Topping, ed., Civil-Comp Press, Stirlingshire, U.K.

Germain, P. (1973). "The method of virtual power in continuum mechanics. Part 2: Microstructure." *SIAM J. Appl. Math.*, 25(3), 556–575.
Greco, L., and Cuomo, M. (2016). "An isogeometric implicit G1 mixed finite element for Kirchhoff space rods." *Comput. Methods Appl. Mech. Eng.*, 298, 325–349.
Javili, A., dell'Isola, F., and Steinmann, P. (2013). "Geometrically nonlinear higher-gradient elasticity with energetic boundaries." *J. Mech. Phys. Solids*, 61(12), 2381–2401.
Lazar, M. (2013). "The fundamentals of non-singular dislocations in the theory of gradient elasticity: Dislocation loops and straight dislocations." *Int. J. Solids Struct.*, 50(2), 352–362.
Lazar, M., and Maugin, G. A. (2006). "Dislocations in gradient elasticity revisited." *Proc. R. Soc. London A: Math. Phys. Eng. Sci.*, 462(2075), 3465–3480.
Lazar, M., Maugin, G. A., and Aifantis, E. C. (2006). "Dislocations in second strain gradient elasticity." *Int. J. Solids Struct.*, 43(6), 1787–1817.
Lekszycki, T., Olhoff, N., and Pedersen, J. J. (1992). "Modelling and identification of viscoelastic properties of vibrating sandwich beams." *Compos. Struct.*, 22(1), 15–31.
Mindlin, R. D. (1965). "Second gradient of strain and surface-tension in linear elasticity." *Int. J. Solids Struct.*, 1(4), 417–438.
Mindlin, R. D. (1972). "Elasticity, piezoelectricity and crystal lattice dynamics." *J. Elast.*, 2(4), 217–282.
Mousavi, S. M. (2016a). "Dislocation-based fracture mechanics within nonlocal and gradient elasticity of bi-Helmholtz type—Part I: Antiplane analysis." *Int. J. Solids Struct.*, 87, 222–235.
Mousavi, S. M. (2016b). "Dislocation-based fracture mechanics within nonlocal and gradient elasticity of bi-Helmholtz type—Part II: Inplane analysis." *Int. J. Solids Struct.*, 92, 105–120.
Peerlings, R. H. J., Massart, T. J., and Geers, M. G. D. (2004). "A thermodynamically motivated implicit gradient damage framework and its application to brick masonry cracking." *Computer Methods Appl. Mech. Eng.*, 193(30), 3403–3417.
Pideri, C., and Seppecher, P. (1997). "A second gradient material resulting from the homogenization of a heterogeneous linear elastic medium." *Contin. Mech. Thermodyn.*, 9(5), 241–257.
Pignataro, M., Ruta, G., Rizzi, N., and Varano, V. (2009). "Effects of warping constraints and lateral restraint on the buckling of thin-walled frames." *ASME 2009 Int. Mechanical Engineering Congress and Exposition*, ASME, New York, 803–810.
Placidi, L. (2015). "A variational approach for a nonlinear 1-dimensional second gradient continuum damage model." *Continuum Mech. Thermodyn.*, 27(4), 623–638.
Placidi, L. (2016). "A variational approach for a nonlinear one-dimensional damage-elasto-plastic second-gradient continuum model." *Continuum Mech. Thermodyn.*, 28(1), 119–137.
Placidi, L., Andreaus, U., Della Corte, A., and Lekszycki, T. (2015). "Gedanken experiments for the determination of two-dimensional linear second gradient elasticity coefficients." *Zeitschrift für angewandte Mathematik und Physik*, 66(6), 3699–3725.
Placidi, L., Andreaus, U., and Giorgio, I. (2016). "Identification of two-dimensional pantographic structure via a linear D4 orthotropic second gradient elastic model." *J. Eng. Math.*, 10.1007/s10665-016-9856-8, 1–21.
Polizzotto, C. (2016). "A note on the higher order strain and stress tensors within deformation gradient elasticity theories: Physical interpretations and comparisons." *Int. J. Solids Struct.*, 90, 116–121.
Rizzi, N., and Varano, V. (2011). "On the postbuckling analysis of thin-walled frames." *13th Int. Conf. on Civil, Structural and Environmental Engineering Computing*, Civil-Comp Press, Stirlingshire, U.K.
Scerrato, D., Giorgio, I., and Rizzi, N. L. (2016a). "Three-dimensional instabilities of pantographic sheets with parabolic lattices: Numerical investigations." *Zeitschrift für angewandte Mathematik und Physik*, 67(3), 1–19.
Scerrato, D., Zurba Eremeeva, I. A., Lekszycki, T., and Rizzi, N. L. (2016b). "On the effect of shear stiffness on the plane deformation of linear second gradient pantographic sheets." *Zeitschrift für Angewandte Mathematik und Mechanik*, in press.
Seppecher, P., Alibert, J.-J., and dell'Isola, F. (2011). "Linear elastic trusses leading to continua with exotic mechanical interactions." *J. Phys.: Conf. Ser.*, 319(1), 012018.
Shodja, H. M., Ahmadpoor, F., and Tehranchi, A. (2012). "Calculation of the additional constants for fcc materials in second strain gradient elasticity: Behavior of a nano-size Bernoulli-Euler beam with surface effects." *J. Appl. Mech.*, 79(2), 021008.
Turco, E., dell'Isola, F., Cazzani, A., and Rizzi, N. L. (2016). "Hencky-type discrete model for pantographic structures: Numerical comparison with second gradient continuum models." *Zeitschrift für angewandte Mathematik und Physik*, 67(4), 1–28.
Yang, Y., and Misra, A. (2010). "Higher-order stress-strain theory for damage modeling implemented in an element-free Galerkin formulation." *Comput. Modell. Eng. Sci.*, 64(1), 1–36.
Yang, Y., and Misra, A. (2012). "Micromechanics based second gradient continuum theory for shear band modeling in cohesive granular materials following damage elasticity." *Int. J. Solids Struct.*, 49(18), 2500–2514.